Physicochem. Probl. Miner. Process., 61(1), 2025, 200063

http://www.journalssystem.com/ppmp

Physicochemical Problems of Mineral Processing

ISSN 1643-1049

Effect of column segment diameter ratio on flow field and separation performance of the composite column-cone hydrocyclone

Peikun Liu [1], Xiangxi Xu [1], Xinghua Yang [1], Anjun Li [1], Bo Chen [1], Gang Liu [2], Yunzhu Gao[2]

[1] College of Mechanical and Electronic Engineering, Shandong University of Science and Technology, Qingdao 266590, China

[2] Shandong Xinjulong Energy Co., Ltd, Heze 274900, China

Corresponding author: lianjun@sdust.edu.cn (Anjun Li)

Abstract: To address the misplacement of fine particles in the underflow caused by structural defects in conventional hydrocyclones, a composite column-cone hydrocyclone (C-C hydrocyclone) was proposed, featuring a cone-column-cone structure. Computational Fluid Dynamics (CFD) techniques were employed to study the diameter ratio and various configurations of C-C hydrocyclone, assessing the impact on separation performance. Results indicated that increasing the column section diameter ratio from 0.5 to 0.7 reduced the cutting size by 22.96 %, enhanced sharpness by 9.87 %, and improved separation efficiency. These findings offer valuable insights for the design and application of C-C hydrocyclones based on specific requirements such as grinding classification and flotation operations.

***Keywords*:** hydrocyclone, diameter ratio, numerical simulation, separation performance

1. Introduction

Hydrocyclone is a kind of equipment that utilizes centrifugąal force to realize solid-liquid or liquid-liquid separation, which is widely used in petroleum, chemical, mining and other industries (Song et al., 2020; Xie et al., 2020; Li et al., 2021; Zhou et al., 2023). However, due to the inherent defects in the structure of the conventional hydrocyclone, the internal flow field is unstable, which affects the particle trajectory, resulting in difficult control of its separation sharpness and cutting size. These factors often lead to the misplacement of fine particles in the underflow. The phenomenon of ore over-grinding (Jiang et al., 2020) in the application of grinding and classifying operation often causes the problems of lower product throughput (Lee et al., 2020) and higher energy consumption (Dundar, 2020), thus increasing the production cost of the coal processing plant. Therefore, in order to optimize the structure design, many works have been carried out to study the relationship between structure and separation performance.

Changing the boundary structure of the cone section will directly affect its internal flow field and particle motion characteristics. It is now recognized that the cone angle and cone cross-section shape are the key parameters of the cone structure. The numerical results of single cone hydrocyclone show that increasing the cone angle can improve the tangential velocity and pressure gradient, but it will reduce the separation efficiency. Fu (2022) investigated the influence law of cone angle size on the separation performance of hydrocyclone, and found that the cutting size is gradually increased as the cone angle increases. The hydrocyclone with small cone angle is more conducive to the separation of fine particles, while large cone angle is more suitable for the separation of high concentration with coarse particles. When the cone angle is close to 180°, the flat-bottom hydrocyclone is created. Hou et al. (2023) found that an appropriate increase in the diameter of the top of the spigot can improve the separation sharpness and reduce the misplacement of fine particles in the underflow. Compared with single-cone hydrocyclone, composite cone hydrocyclone consisting of multiple tandem cones exhibits different performance with the change of cone angle. However, the effect of the combination form of composite cone hydrocyclone on classification performance has not been uniformly recognized. Yang et al. (2010) found that with a constant second cone angle, the first cone with a larger angle has a higher separation efficiency but leads to more micrometer-sized fine particles into the underflow, contrary to

DOI: 10.37190/ppmp/200063

the effect of the angle change on the separation efficiency in the single-cone hydrocyclone. They also concluded that a smaller cone difference between two conical section is favorable to obtain higher separation accuracy. Ye et al. (2019) designed four types of biconical hydrocyclone, according to the numerical calculation results, the cone segment design of biconical classification hydrocyclone should be composed of a long upper cone with small cone angle and a short lower cone with large cone angle. Jiang et al. (2023) simulated the biconical hydrocyclone with different combinations of conical segments, and analyzed the effects of the combination form and structural parameters on the internal multiphase flow motion and separation efficiency. Their results showed that the total separation efficiency decreased with the increase of the upper cone angle, which contradicted Yang's conclusion (2010). In addition, to mitigate the adverse effects of sudden changes in the cone angle at the intersection of linear composite cones, Motin et al. (2017) designed a hyperbolic cone structure with the concave inward toward the axis, which significantly improved the quality of the overflow product but increased the problem of fine particles in the underflow as compared to linear cones. Liu et al. (2023) developed a parabolic cone structure protruding outward from the axis, found that the effect is opposite to the hyperbolic cone structure. In addition, Jiang et al. (2022) combined the advantages of hyperbolic and parabolic cone structures and designed a composite curved cone structure, which can simultaneously alleviate the problems of coarse particle misplacement in the overflow and fine particle misplacement in the underflow. Different curved cone structures of composite cone hydrocyclone have been widely studied, but due to the difficulty of equipment manufacturing, the linear cone structure is still the main cone form.

Separation space is another important parameter that determines the separation performance of the hydrocyclone. Chu et al. (2004) pointed out that the increase of the space within the conical cross-section will improve the separation performance. In addition, Ghodrat et al. (2016) investigated several different curved cone configurations and found that there exists an optimum point for convex cones, so that either too large or too small an internal space is not reasonable. Vega-Garcia et al. (2018) reported that their design of parabolic walls in a 3D-printed 10 mm hydrocyclone obtained higher solids recoveries than the conventional single cones, which seems to not entirely be consistent with the Ghodrat et al. (2016). Kinetic analyses have shown that the separation performance is the result of a combination of force, residence time and separation space.

However, relatively few studies have examined the effects of column-cone section combination hydrocyclones on the internal flow field and separation efficiency, and their mechanism of action remains unclear. More importantly, there is no quantitative design basis for selecting and matching the structural parameters of the column-cone combination hydrocyclone, which serves as the basis for this study. Given these complexities, this study employs numerical simulations to systematically investigate the effects of different lower column diameters and their combinations on the flow characteristics and separation performance of column-cone (C-C) hydrocyclones. The results are significant for reducing the misplacement of fine particles in the underflow and for designing C-C hydrocyclones for special applications.

2. Mathematical model

2.1. Geometric structure

As shown in Fig. 1, compared with conventional hydrocyclone, C-C hydrocyclone is able to reduce the accumulation of particles at the bottom of the cone section. The coercion of coarse particles to fine particles has also been reduced, and the distribution of coarse and fine particles in the radial direction is more reasonable.

The diameter ratio refers to the ratio of the diameter of the lower column section to the diameter of the upper column section. The radial settling distance of particles in C-C hydrocyclone is significantly affected by the diameter of the lower column section. It is directly related to the trajectory of particles and the separation space. Since too small a diameter ratio will block the flow field and too large a diameter ratio will make the flow field unstable, the range of diameter ratios proposed in this paper is 0.4 - 0.7. Changes in the diameter ratio are accompanied by alterations in the upper and lower cone angles. When the cone angle of a hydrocyclone is modified, its separation performance undergoes significant changes. The reasons for this are varied. On one hand, the radial travel distance of particles

becomes shorter, facilitating their settlement on the wall. On the other hand, the overall separation space of the hydrocyclone decreases, leading to a reduced effective residence time. However, it remains unclear which factor predominates. Therefore, for C-C hydrocyclone, the separation performance is regulated by the upper conical section, lower column section and lower conical section together. Therefore, it is necessary to study the diameter ratio in many different combinations of forms

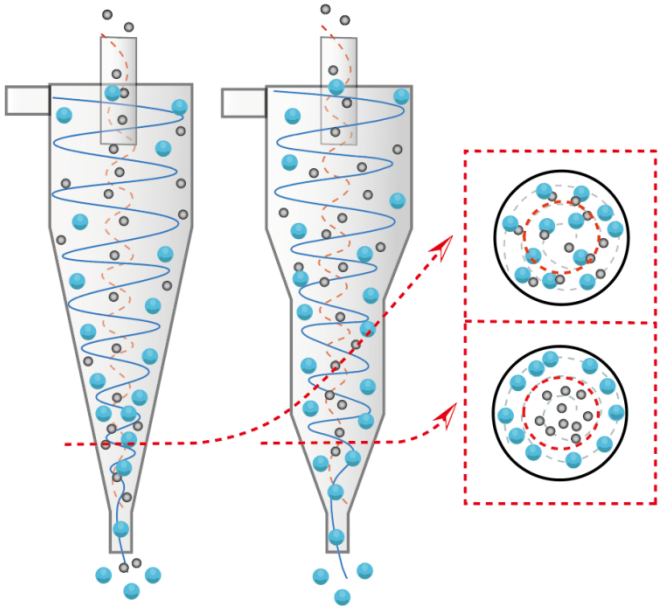

Fig. 1. Separation principle

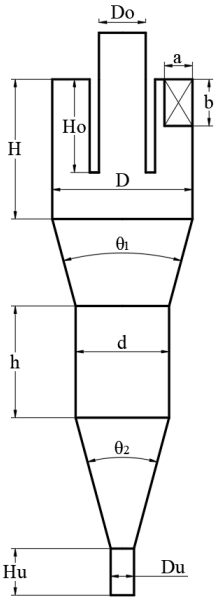

Fig. 2. Structural parameters of C-C hydrocyclone

Structural design based on the laboratory Φ 75 mm hydrocyclone is shown in Fig. 2. The specific structural parameters are shown in Table. 1. The structure is divided into 8 types according to the different combination methods and diameter ratios of C-C hydrocyclone, as shown in Fig. 3. The specific conical cross-section parameters are shown in Table. 2. According to the different diameter ratios, it can be divided into four types: I, II, III and IV. The minimum diameter ratio of type I is 0.5, and the maximum diameter ratio of type IV is 0.8. Meanwhile, on the basis of keeping the total height unchanged, the upper and lower cone angles of type A structure remain unchanged, but with the increase of the diameter ratio, the upper cone section gradually becomes shorter and the lower cone

section gradually becomes longer. Type B structure ensures that the axial position of the lower column section remains unchanged, which leads to a gradual decrease in the upper cone angle and a gradual increase in the lower cone angle with the increase of the diameter ratio.

Table 1. Structural dimensions of C-C hydrocyclone

Structure parameters	Size
Body diameter D/mm	75
Size of inlet a×b/mm	15×25
Height of upper column H/mm	75
Height of lower column H/mm	60
Diameter of lower column d/mm	37.5 ; 45 ; 52.5 ; 60
Diameter of spigot Du/mm	12.5
Diameter of overflow Do/mm	25
Height of vortex finder Ho/mm	50
Height of spigot /mm	25

Table 2. Structural parameters of the conical section

Hydrocyclone	Diameter of lower cylinder section d[mm]	Upper cone θ1[°]	Lower cone θ2[°]
A-I	37.5	35	35
A-II	45	35	35
A-III	52.5	35	35
A-IV	60	35	35
B-I	37.5	43	27
B-II	45	35	35
B-III	52.5	26.5	42.5
B-IV	60	18	49.5

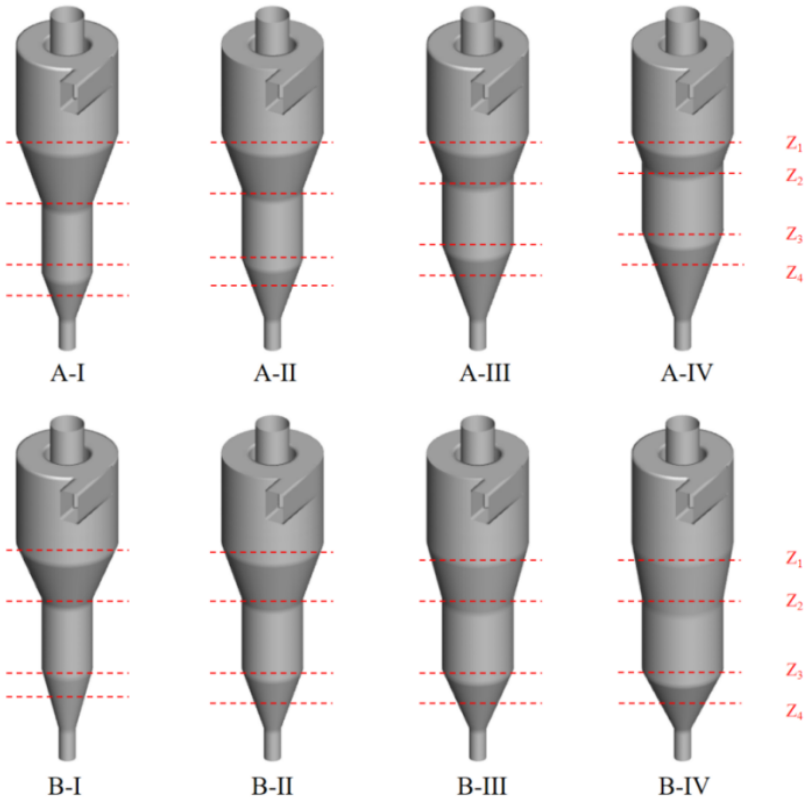

Fig. 3. The C-C hydrocyclone with different structures

In order to accurately analyze the structure, four cross-sections are selected for analysis: cross-section Z_1 is the interface between the upper column section and the upper conical section; cross-section Z_2 is the interface between the upper conical section and the lower column section; cross-section Z_3 is the interface between the lower column section and the lower conical section; cross-section Z_4 is 10mm below the intersection of the lower conical section and the lower column section.

2.2. Model description

Considering the complexity of the multiphase flow field inside C-C hydrocyclone, the simulation process is divided into two steps. The first step is to use the RSM turbulence model and Volume of Fluid (VOF) model to obtain a stable gas-liquid two phase flow field and a stable air column, and to analyze its pressure field and velocity field. The second step is to change the VOF model to Mixture model to calculate the gas-liquid-solid three phase flow field to predict the separation performance of C-C hydrocyclone after the flow field is stabilized. The solid particles with different size distributions will be addded aiming to study the effect of different column section diameter ratios on the particle classification effect.

2.2.1. RSM model

The RSM model removes the assumption of isotropic turbulent viscosity, comprehensively considers the rapid changes of fluid vortices, rotations and other rapid changes. The accuracy will be higher in the prediction of the complex flow field. Meanwhile, comprehensively takes into account the anisotropy of turbulent flow, which is more suitable for the numerical simulation of the hydrocyclone. This model is able to take into account complex interactions in the turbulent field, such as directional effects, but this also means that it is computationally more complex and time-consuming. The RSM is chosen to carry out the solution calculations, taking into account the advantages of RSM in the efficiency of the calculations and the compatibility with Mixture.

The RSM turbulence model control equations is:

$$\frac{\partial\left(\rho\overline{u_i'u_j'}\right)}{\partial t}+\frac{\partial\left(\rho u_k\overline{u_i'u_j'}\right)}{\partial x_k}=D_{T,ij}+D_{L,ij}+P_{ij}+G_{ij}+\varphi_{ij}+\varepsilon_{ij}+F_{ij} \quad (1)$$

where, $\rho\overline{u_i'u_j'}$ is the mean Reynolds stress; $D_{T,ij}$ is the turbulent kinetic energy dispersion term; $D_{L,ij}$ is the molecular viscous diffusion term; P_{ij} is the shear generation term; G_{ij} is the buoyancy generation term; φ_{ij} is the pressure strain term; ε_{ij} is the viscous dissipation term; F_{ij} is the rotational generation term of the fluid; ρ、u_k is the density and viscosity of the fluid. Note that the RSM mixed turbulence option is used in this study, where the phases share the same turbulent field.

2.2.2. VOF model

The VOF model is suitable for the solution of two-phase or multiphase fluids that are immiscible. Based on this property, this simulation study of gas-liquid two-phase flow inside the hydrocyclone, the velocity field characteristics obtained are in good agreement with the LDV measurement results. But in some cases, the VOF method has difficulties in providing mesh convergence of the interfacial area, which may affect the accuracy of multiphase flow simulations. The simulated fluid domain is filled by each phase fluid. The control volume occupied by each phase fluid is the volume fraction of the simulated fluid domain, which sums up to 1.

$$\sum_{q=1}^{n}\alpha_1=1 \quad (2)$$

where $\alpha_q$is the volume fraction of the phase qth within the fluid microelement.

2.2.3. Mixture model

The Mixture model predicts the discrete phases by mixing the term momentum equation and the continuity equation, which belongs to one of the simplified models of Eulerian multiphase flow. It is suitable for cases where the distribution of the dispersed phases is more centralized or where the inter-phase tracing law is not known, but if accuracy is required, the TFM model is a better choice. It has strongly coupled and can simulate multiphase flow with different velocities between the phases. It can

describe the flow field distribution of multiphase fluid mixing, and the accuracy of the model has been verified by many scholars.

Multiphase flow modeling continuity equations:

$$\frac{\partial}{\partial t}(\rho_m) + \nabla(\rho_m \vec{v}_m) = 0 \quad (3)$$

where: ρ_m is the mixed-phase density; t is the time; ∇ is the Laplace operator; and $\vec{v}_m$ is the mixed-phase average velocity.

Its momentum conservation equation is:

$$\frac{\partial}{\partial t}(\rho_m \vec{v}_m) + \nabla(\rho_m \vec{v}_m \vec{v}_m) = -\nabla \cdot \vec{p} + \nabla \cdot \left[\mu_m\left(\nabla v_m + \nabla \vec{v}_m{}^T\right)\right] + \rho_m \vec{g} + \vec{F} + \nabla \cdot \left(\sum_{k=1}^{N} \alpha_k \rho_k \vec{v}_k{}^r \vec{v}_k{}^r\right) \quad (4)$$

where $\vec{p}$ is the pressure; $\vec{F}$ is the volume force; μ_m is the mixed phase density; ρ_k is the kth phase density; N is the total number of phases; and $v_k{}^r$ is the relative slip velocity of the kth phase and the mixed phase.

2.3. Simulation condition

During the simulation process, the transient pressure solver in Fluent 2021R1 software was employed to evaluate and compare the separation performance and flow field characteristics of column-cone hydrocyclones with different structures under identical working conditions. Mesh generation was conducted using ICEM 18.0 software. The numerical simulations utilized approximately 2.0×10^5 mesh elements, with a maximum mesh size of 2.6 mm. The inlet boundary condition is set as "velocity inlet", with an velocity of 4.5 m/s. The spigot and vortex finder are set as "pressure outlet". The air-phase return volume fraction is set as 1. The boundary condition of hydrocyclone wall is "No-slip". The pressure-velocity coupling is performed by the "SIMPLE" algorithm. The pressure discretization format is "PRESTO!". The momentum discretization format is "QUICK". The time step is set to 1.0×10^{-5}, and the balance of mass flow in each phase at the inlet and outlet is taken as the convergence condition. In order to simulate the actual hydrocyclone conditions, the main phase in the Mixture model is set to be water phase, and the air phase is added at the same time. The solid particles are quartz particles with the density of 2650 kg/m^3. The particles are continuously distributed. In the simulation, the total solid phase concentration is 10 % by mass ratio, which is converted to get the total volume fraction of solids as 4 %. The material used in the experiment is divided into 9 particle size segments, as shown in Table 3.

Table 3. Particle size distribution

Mean size/μm	1	5	10	15	22	30	44	60	80	Total
Yield/%	4.35	8.47	9.95	12.35	18.17	15.8	14.32	9.82	6.73	99.96
Volume fraction/%	0.174	0.339	0.398	0.494	0.727	0.632	0.573	0.393	0.271	4.001

2.4. Model validation

The simulation models are validated by comparing the velocity distribution and separation behavior of the hydrocyclone between our lab and Hsieh's (1998) work. The comparison of tangential and axial velocities for the 60 mm section below the top cover of the Φ 75 mm hydrocyclone is shown in Fig. 4(a) and 4(b). From the comparative analysis of the figures, it can be seen that the simulation results obtained are basically consistent with the experimental results. The difference shown at the maximum value of tangential velocity is mainly caused by the practical application of model and experimental errors. The RSM model is validated by the work of Hsieh at a feed solids concentration of 4.01% by volume as well as the home-measured data under the same conditions as the simulation (20° single cone). Fig. 4(c) displays the comparison of the grading efficiency curves of the experiment and simulation, which has the same trend of change with an error of less than 5 %. However, the measured recovery of fine particles (<4 μm) is zero in Fig. 4(c), whereas the predicted recovery is close to the water split ratio. Due to the strong following behaviors of fine particles, the predicted results should be more reasonable. Overall, it can be concluded that current models can adequately predict the flow field and separation performance of the hydrocyclone.

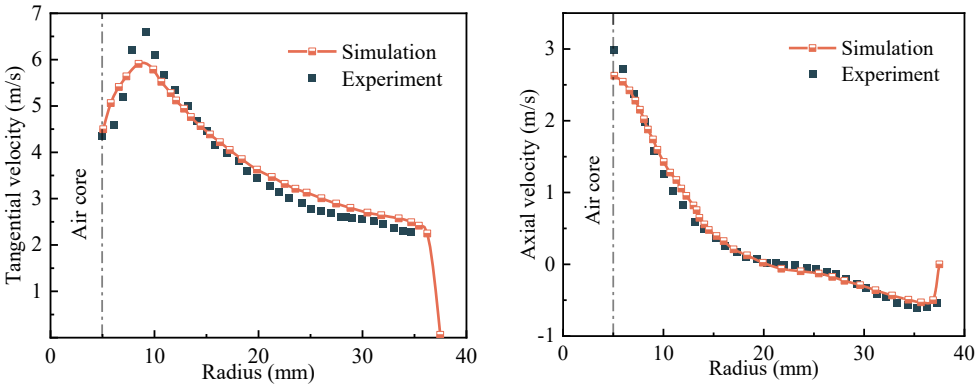

(a) The tangential velocity (b) The axial velocity

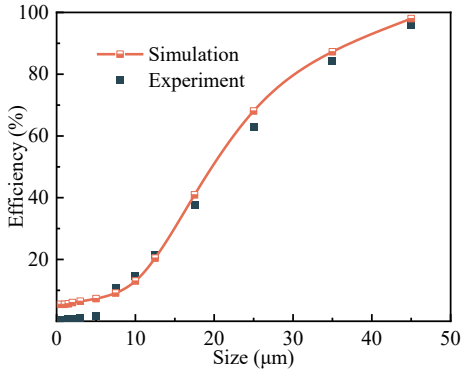

(c) Particle separation performance

Fig. 4. Validation of the model

3. Results and discussion

3.1. Pressure

Fig. 5 shows the cloud diagram of pressure distribution in the cross-section of C-C hydrocyclone with different diameter ratio. It can be seen that the pressure distribution on the centre section still maintains a good symmetry, indicating that the radial pressure distribution law within the flow field of C-C hydrocyclone is not affected by the change of the diameter ratio. Combined with Fig. 7, in the $Z_2 \sim Z_3$ section where the lower column section is located, the pressure of A-III type hydrocyclone decreases from 105.57 K to 104.15 K from top to bottom, which is a decrease of 1.3 %. The maximum pressure on the wall surface does not change much, which indicates that the lower column section has the effect of stabilizing the flow field. But a small diameter ratio of the lower column section is bad for the stability of the flow field, such as B-I type, from 97.04 kPa at the Z_2 cross-section to 91.02 kPa at the Z_3 cross-section, a reduction of 6.2 %. The degree of change in pressure along the axial direction is much larger than the structure of type III, indicating that too small diameter ratio will produce the role of blocking the flow field, which is not conducive to the stabilisation of the flow field.

The maximum pressure drop of the hydrocyclone is directly proportional to its energy consumption. Reducing the pressure drop can improve the processing capacity of the hydrocyclone to a certain extent. Fig. 6 illustrates the pressure drop comparison between Type A and Type B hydrocyclones. When the diameter ratio is 0.7, the pressure drop difference between the two hydrocyclone configurations is significant. The pressure drop in Type B is reduced by 15.52 % compared to Type A, attributed to alterations in the upper and lower cone angles resulting from a change in configuration. This indicates that the cone angle significantly influences the pressure change. Generally, the pressure drop decreases with an increasing diameter ratio. However, when the diameter ratio for the Type B structure reaches 0.8, the pressure drop increases by 8.92 % compared to a diameter ratio of 0.7, and the stability of the flow field decreases. This may be due to an increase in the lower cone angle. Thus, the diameter ratio should not be excessively large.

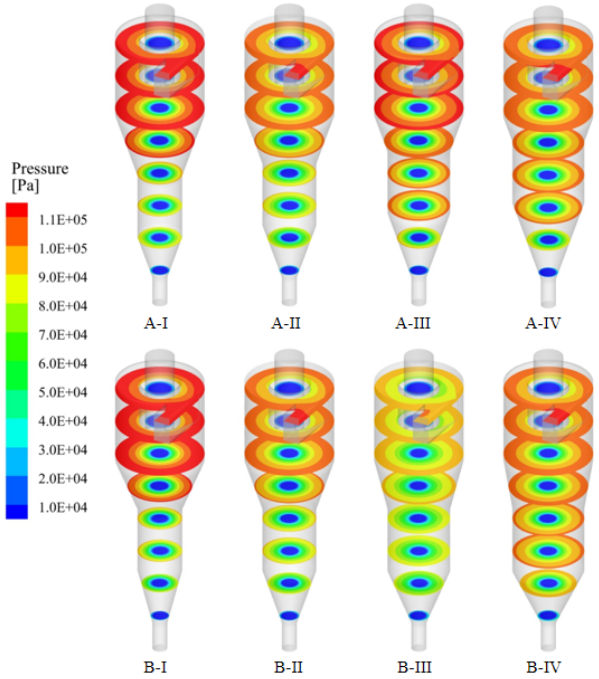

Fig. 5. Contour of the pressure distributions

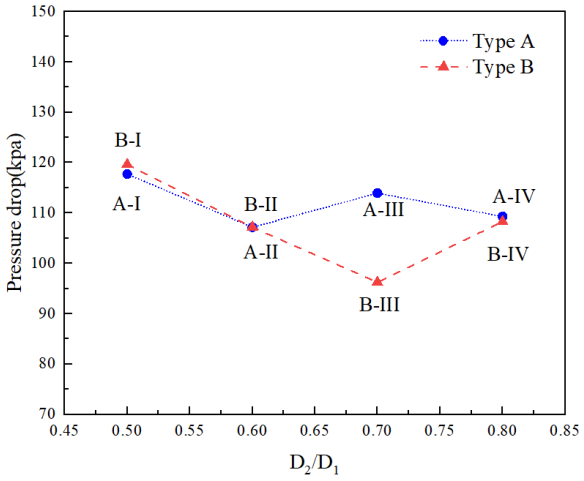

Fig. 6. Pressure drop

In order to accurately analyse the effect of the diameter ratio on the static pressure within the flow field of C-C hydrocyclone, the static pressures at each cross-section are considered. In Fig. 7, the static pressure shows a decreasing trend along the radial direction from the wall to the centre position, and the pressure gradient decreases sharply near the air core due to the transformation of the pressure energy into kinetic energy. The internal pressure continues to decrease until the formation of a negative pressure, which manifests itself as a negative value at the forced vortex. The observed phenomenon may be attributed to changes in the hydrocyclone's internal fluid space when the diameter ratio is altered. The maximum static pressure at the wall is inversely proportional to the size of this space: the smaller the space, the higher the static pressure at the wall. For instance, in the Type A structure, as the diameter ratio increases from 0.5 to 0.8, the maximum wall pressure at section Z_1 decreases from 117.59 kPa to 109.21 kPa, a reduction of 7.12 %.

Altering the combination significantly affects the static pressure at the wall of a C-C hydrocyclone when the diameter ratio is 0.7. The maximum pressure drop decreases from 113.34 kPa to 96.14 kPa, a reduction of 15.18 %, due to a decrease in the upper cone angle from 35° in Type A to 26.5° in Type B. This indicates that reducing the upper cone angle helps decrease pressure. In conventional

hydrocyclones, the maximum pressure drop typically decreases with an increase in separation space. However, in C-C hydrocyclones, pressure is determined by the combined regulation of the upper and lower cone angles and the separation space. As the parameter variations in this study primarily involve the diameter ratio, the radial pressure gradient is more significantly influenced by the diameter of the lower column section. The pressure drop and radial pressure gradient are smallest in the B-III structure and largest in the B-I structure.

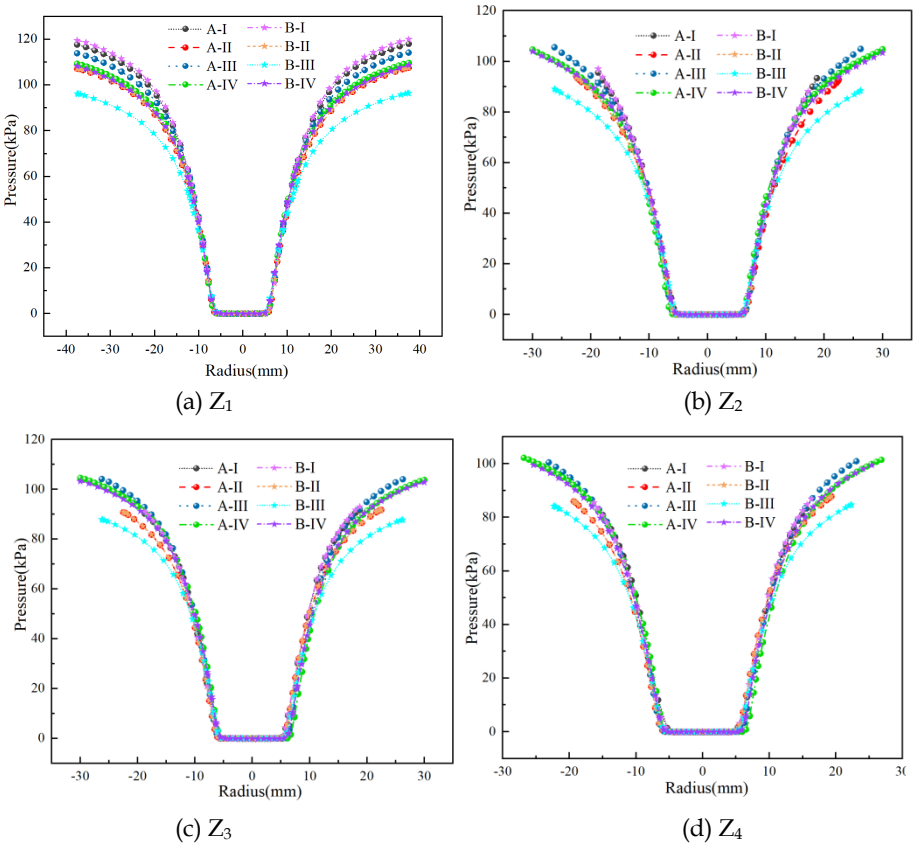

(a) Z_1 (b) Z_2

(c) Z_3 (d) Z_4

Fig. 7. Comparison of the radial pressure distributions

3.2. Tangential velocity

Fig. 8 shows the effect of different diameter ratios on the tangential velocity distribution for the two combined forms. The tangential velocity inside C-C hydrocyclone also shows a symmetric distribution, which first increases sharply along the radial direction from the centre point and reaches the maximum value near the radial position r = 7.5 mm. Then it decreases gradually along the increase of radial position and finally decreases rapidly to zero near the wall, which obeys the velocity distribution law of the combined vortex.

It can be found that with the increase of diameter ratio, the tangential velocity of type A structure shows an overall trend of decreasing, while type B structure shows an overall trend of decreasing first and then increasing. When the diameter ratio is 0.5 and 0.6, the magnitude and trend of tangential velocity of type A structure and type B structure are almost the same at each section, which indicates that when the diameter ratio is too small, the change of the combination form does not have a significant effect on the tangential velocity. When the diameter ratio is too large, such as the tangential velocity of type IV hydrocyclone shows a trend of increasing again. Using the Z_1 cross-section of type B structure as an example, when the diameter ratio increases from 0.5 to 0.7, the maximum tangential velocity decreases from 10.56 m/s to 9.33 m/s, with a decrease of 11.64 %. When the diameter ratio increases from 0.7 to 0.8, the tangential velocity increases from 9.33 m/s to 10.26 m/s, with an increase of 9.97 %.

However, when the diameter ratio is 0.7 (type III structure), from type A to type B, at Z_1 cross-section, the tangential velocity decreases from 10.59 m/s to 9.33 m/s, with a decrease of 11.9 %. At Z_2 cross-section, it decreases from 10.99 m/s to 9.33 m/s, with a decrease of 10 %. At Z_3 cross-section, it decreases

from 10.94 m/s to 9.91 m/s, with a decrease of 9.41 %. At Z_4 cross-section, it decreases from 10.78 m/s to 10 m/s, a decrease of 7.23 %. It can be found that the tangential velocity reduction decreases as the cross-section position goes down, indicating that the tangential velocity is more influenced by the regulation of the upper cone section at this diameter ratio.

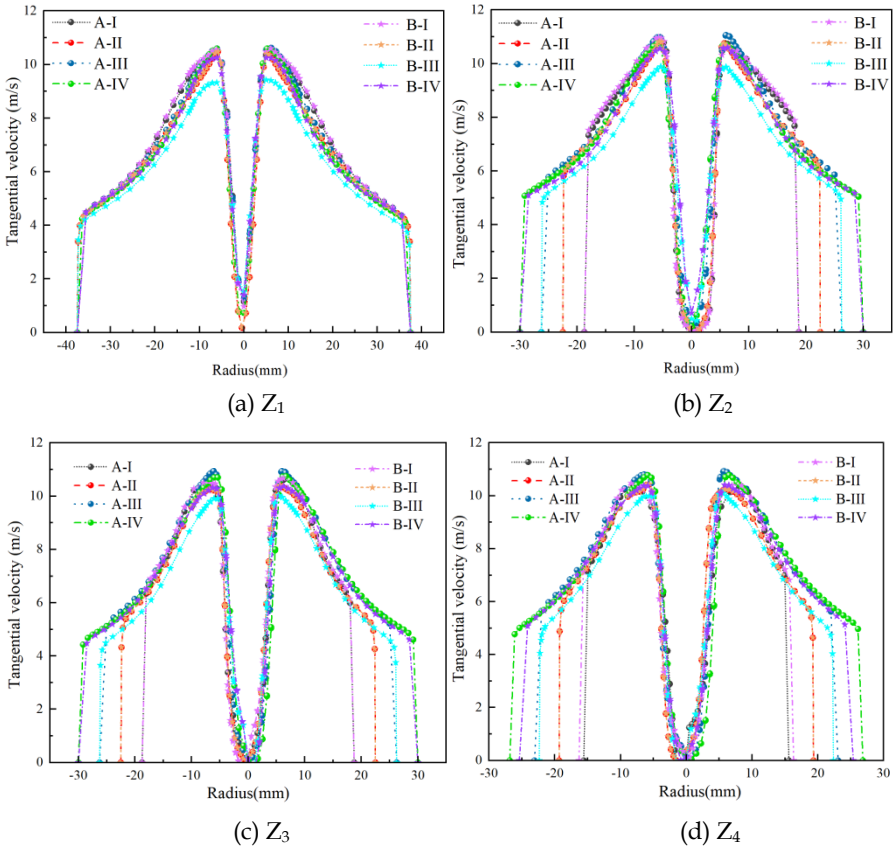

Fig. 8. Comparison of the tangential velocity distributions

3.3. Axial velocity

The fluid distribution within a hydrocyclone is closely linked to axial motion. As illustrated in Figure 9, the influence of the diameter ratio on the axial velocity distribution and fluid motion trajectory is more clearly observed. Arrows indicate the direction of fluid movement. The zero-velocity envelope divides the axial motion into an upward inner swirl (red area) and a downward outer swirl (blue area). The figure shows that while an increase in the diameter ratio does not alter the distribution pattern of the zero-velocity envelope, it does increase the area of the internal swirl. The closed area beneath the lid indicates the presence of circulating flow within the flow field. Some researchers suggest that this circulating flow facilitates secondary separation, aiding in the re-separation of coarse particles misplaced in the internal cyclonic flow and reducing the content of particles in the short-circuit flow.

Combined with Fig. 10, it can be found that the zero-velocity envelope at the Z_1 section is less affected by the structural changes, and the radius of zero-velocity envelope fluctuates in the range of 40 mm ~ 45 mm. The diameter of zero-velocity envelope at the Z_2 and Z_3 sections is mainly affected by the diameter ratio, in combination with the corresponding wall radius of each section of the lower column section, it can be found that the radial position of the zero velocity envelope is about 65 % ~ 70 % of the radius of each section.

The magnitude of the axial velocity determines the residence time of the particles in the hydrocyclone, which is one of the important indexes for evaluating the separation performance of the hydrocyclone. The axial velocities distributed along the radial direction of C-C hydrocyclone were analyzed separately. The results are shown in Fig. 10. It can be found that the change rule of type A and type B structure in the outer swirl region is almost the same, indicating that the change of combination mode has no significant effect on the axial velocity in the outer swirl region.

The changes of diameter ratio and combination method have limited influence on the axial velocity distribution along the Z_1 axis. In contrast, the diameter ratio significantly affects the axial velocity distribution along the Z_2, Z_3 and Z_4 axes. The axial velocity in the outer swirl region decreases with increasing diameter ratio. The axial velocity in the inner swirl region increases with increasing diameter ratio along the Z_2 axis, but decreases with increasing diameter ratio at Z_3 and Z_4. The magnitude of change in axial velocity is greater for type A structure than type B.

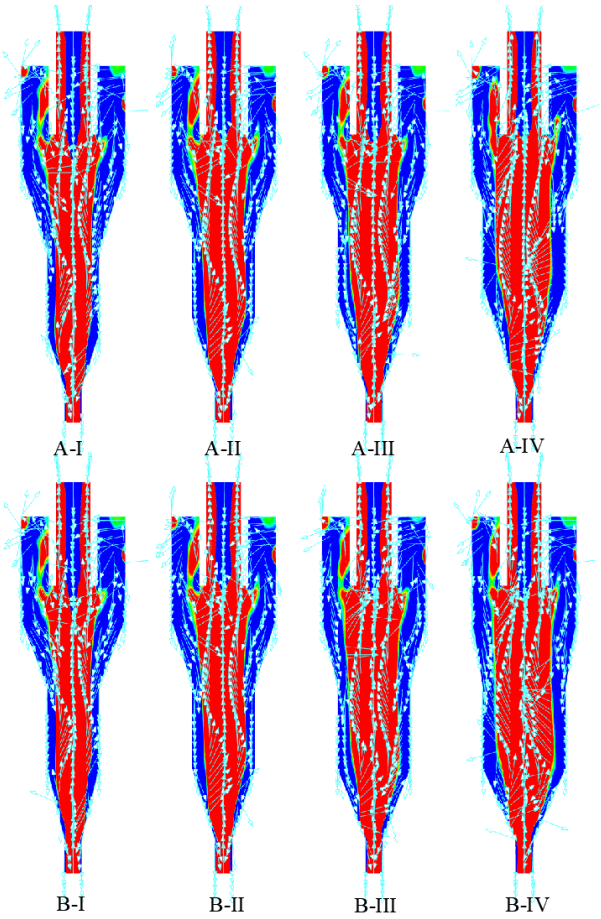

Fig.9. Contours of the axial velocity distributions

3.4. Separation efficiency

Fig. 11 shows the comparison of separation efficiency curves of conventional hydrocyclone and different C-C hydrocyclones. Each point on the efficiency curve represents the recovery rate of the corresponding particle size in the underflow. Therefore, the efficiency curve reflects the relationship between the distribution of various types of particles, which is a key indicator for evaluating the separation performance of hydrocyclone.

Compared with the conventional hydrocyclone, the content of fine particles below 20 μm in the underflow of C-C hydrocyclone is significantly reduced. Compared with the fine particles and coarse particles, the effect of the diameter ratio on the underflow recovery of particles with a particle size of 20 μm - 60 μm is much larger. When the diameter ratio increases, the efficiency curve moves upward, indicating that the classification efficiency of each particle increases. However, the separation efficiency will be lower when the diameter ratio increases to 0.8.

In the Type B structure, increasing the diameter ratio results in a decrease in the upper cone angle and an increase in the lower cone angle. At a diameter ratio of 0.7, there is a significant misplacement of fine particles. Additionally, when the diameter increases from 15 mm to 20 mm, the classification efficiency for 30 μm particles drops from 54.54 % to 19.68 %. This indicates that a decrease in the upper cone angle has a substantial impact on separation efficiency.

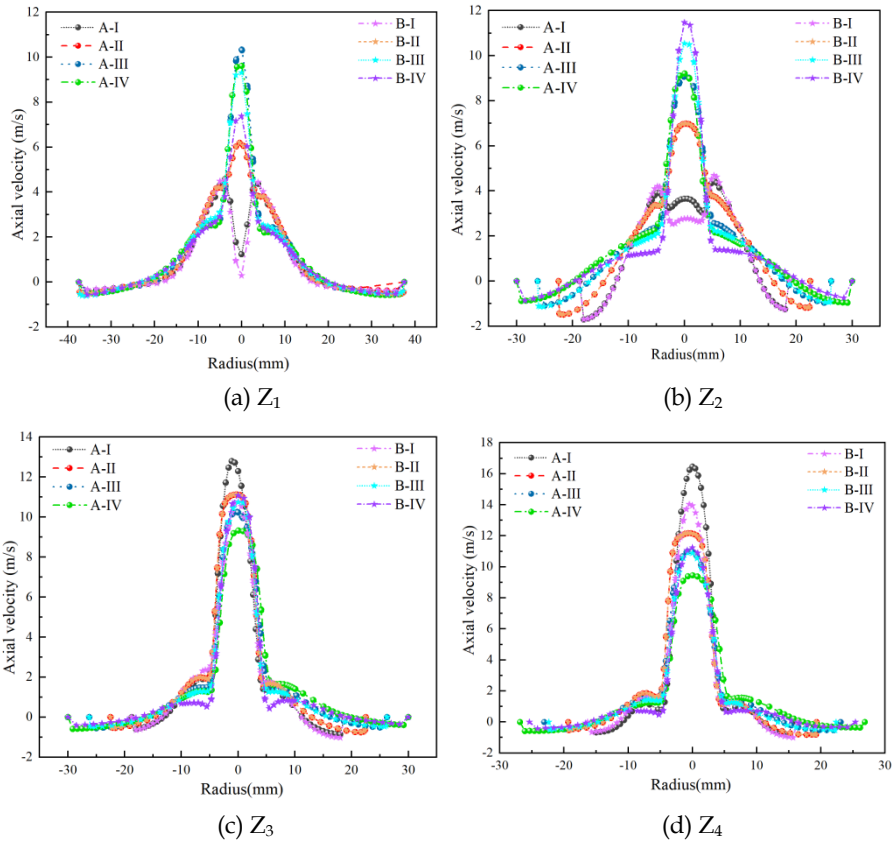

(a) Z_1 (b) Z_2

(c) Z_3 (d) Z_4

Fig. 10. Comparison of the axial velocity distributions

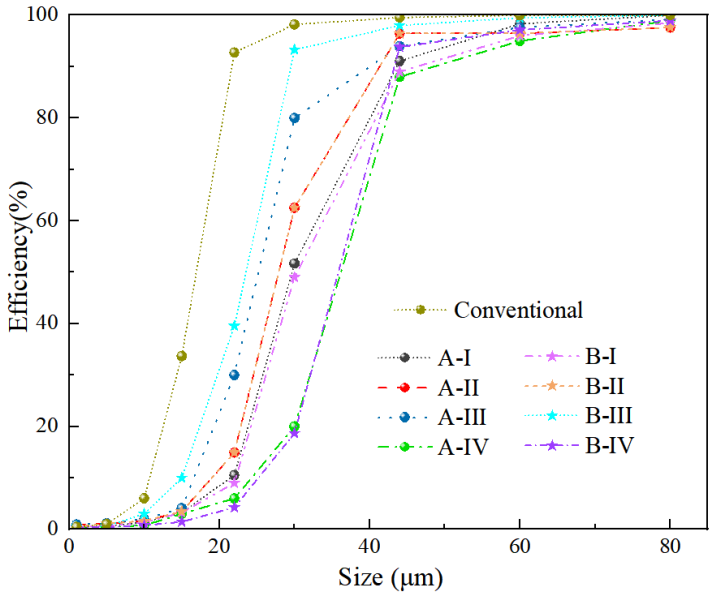

Fig. 11. Separation efficiency

The most important characteristic indexes for evaluating the efficiency curve are the cutting size d_{50} and the separation accuracy α. The classification accuracy α is obtained from the slope of the efficiency curve (sharpness index) S.

$$S = \frac{d_{25}}{d_{75}} \tag{5}$$

The efficiency curve analysis results are presented in Fig. 12. As the diameter ratio increases from 0.5 to 0.7, the cutting size for the Type A structure decreases from 29.76 μm to 25.33 μm, while for Type

B, it decreases from 30.44 μm to 23.45 μm, demonstrating an overall decreasing trend. However, when the diameter ratio increases to 0.8, the cutting size increases, indicating that an excessively large diameter ratio can increase the cutting size. The sharpness generally increases with the diameter ratio. The most notable change is observed at a diameter ratio of 0.7, where the steepness index of the Type B structure decreases by 12.78 % compared to Type A, resulting in poorer separation accuracy. It is concluded that both excessively large and small diameter ratios decrease separation efficiency. Additionally, the angle of the upper cone section significantly impacts separation efficiency.

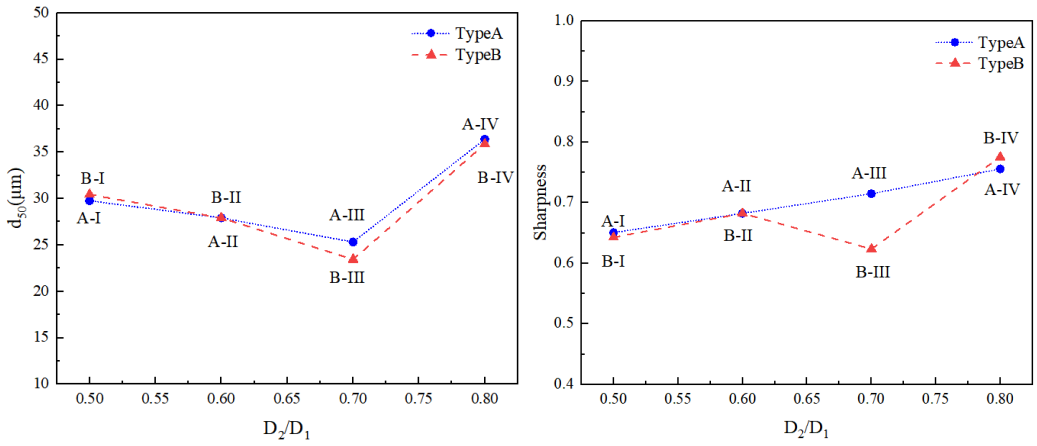

(a) cutting size (b) sharpness

Fig. 12. Separation performance

For the hydrocyclone separation operation, more particles larger than d_{50} and fewer particles smaller than d_{50} in the underflow indicate a better separation result. This expectation can be reflected in the classification efficiency curve by that, in the case of ensuring that the d_{50} meets the production requirements, the greater slope of the curve (the sharpness closer to 1), the greater separation accuracy of the hydrocyclone. From the above study, it can be seen that for C-C hydrocyclone, the small diameter ratio has a large cutting size, a small steepness index, which result in a low separation efficiency. A large diameter ratio has a large steepness index but also a large cutting size, which is prone to produce misplacement of coarse particles in the overflow. Therefore, in this study, A-III structure (when the upper and lower cone angles of C-C hydrocyclone are constant at 35° and the diameter of the lower column section is 0.7) has the highest separation accuracy and the smallest separation size.

4. Conclusions

To enhance the separation accuracy of conventional hydrocyclones and reduce the misplacement of fine particles in the underflow, this paper proposes a composite column-cone hydrocyclone. Numerical simulations were conducted to investigate the effects of varying the diameter ratio of column segments in two configurations (Type A and Type B) on the flow field characteristics and separation performance within a C-C hydrocyclone. The main conclusions are as follows:

(1) Increasing the lower column section in C-C hydrocyclone results in minimal changes to the pressure gradient, tangential velocity, and axial velocity in the lower sections, indicating that this modification helps stabilize the flow field. Compared to conventional hydrocyclones, the content of fine particles in the underflow is significantly reduced.

(2) As the diameter ratio increases, the separation space in C-C hydrocyclone expands, enhancing particle separation and thus improving accuracy. The cutting size tends to decrease. The highest separation efficiency, with a cutting size of 25.33 mm and sharpness of 0.71, is achieved when the diameter ratio is 0.7 and the cone angle remains constant. However, a diameter ratio that is too small can obstruct particle movement, while a ratio that is too large can cause flow field disorder, hindering separation.

(3) The change in combination mode has little effect on C-C hydrocyclone with a small diameter ratio. However, when the diameter ratio is 0.7, the pressure drop in the Type B structure is reduced by

15.52 % compared to the Type A structure. The tangential velocity at the Z1 cross-section decreases by 11.9 %, while the axial velocity remains largely unchanged. This results in the recovery of fine particles in the Type B hydrocyclone being smaller than in Type A. It can be observed from the two combination forms that the separation efficiency of C-C hydrocyclone can be improved by appropriately increasing the upper cone angle and decreasing the lower cone angle at the optimal diameter ratio.

Acknowledgments

Shandong Postdoctoral Science Foundation (No. SDCX-ZG-202400215) and Qingdao Postdoctoral Funding Project (No. QDBSH20230202034) provided financial support for this work.

References

BANERJEE, C., CEPEDA, E., SWITZER, D., HUNTER, S., 2024. *Application potential of cavex® double effect hydrocyclone for the classification of mine tailings - a pilot scale study.* Min Proc Ext Met Rev.

CUI, B.Y., WEI, D.Z., GAO, S.L., LIU, W.G., FENG, Y.Q., 2014. *Numerical and experimental studies of flow field in hydrocyclone with air core.* Trans. Nonferrous. Metals. Soc. 24 (08), 2642–2649.

CHU, L.Y., YU, W., WANG, G.J., ZHOU, X.T., CHEN, W.M., DAI, G.Q., 2004. *Enhancement of hydrocyclone separation performance by eliminating the air core.* Chem. Eng. Process. 43, 1441–1448.

DUNDAR, H., 2020. *Investigating the benefits of replacing hydrocyclones with high-frequency fine screens in closed grinding circuit by simulation.* Miner. Eng. 148, 106212.

FU, S.C., QIAN, Y. X., YUAN, H. X., FANG, Y., 2022. *Effect of cone angles of a hydrocyclone for the separation of waste plastics with low value of density difference*. Waste. Manage. 140: 183-192.

GHODRAT, M., KUANG, S.B., YU, A.B., VINCE, A., BARNETT, G.D., BARNETT, P.J., 2014. *Numerical analysis of hydrocyclones with different conical section designs*. Miner. Eng. 62, 74–84.

GHODRAT, M., KUANG, S. B., YU, A.B., Vince, A., Barnett, G.D., Barnett, P.J., 2014. *Numerical analysis of hydrocyclones with different vortex finder configurations*. Miner. Eng. 63, 125–138.

GHODRAT, M., QI, Z., KUANG, S.B., JI, L., YU, A.B., 2016. *Computational investigation of the effect of particle density on the multiphase flows and performance of hydrocyclone.* Miner. Eng. 90, 55–69.

GUO, Z.Y., SUN, Y.J., PAN, S.Y., CHANG, P.C., 2019. *Integration of green energy and advanced energy-efficient technologies for municipal wastewater treatment plants.* Int. J. Environ. 16(7):1282.

HOU, D.X., CUI, B.Y., ZHANG, H., ZHAO, Q., JI, A.K., WEI, D.Z., FENG, Y.Q., 2021. *Designing the hydrocyclone with flat bottom structure for weakening bypass effect.* Powder. Technol. 394, 724-734.

HOU, D.X., CUI, B.Y., ZHAO, Q., WEI, D.Z., SONG, Z.G., FENG, Y.Q., 2021. *Research on the structure of the cylindrical hydrocyclone spigot to mitigate the misplacement of particles*. Powder. Technol. 387, 61-71.

HOU, D.X., ZHAO, Q, LIU, P.K, JIANG, L.Y., CUI, B.Y., WEI D.Z., 2023. . *Effects of bottom profile on the circulation and classification of particles in cylindrical hydrocyclones.* Adv. Powder. Technol. 34: 7.

HOU, D.X., LIU, P.K., ZHAO, Q., 2023. *Effect of separation space on the separation performance of cylindrical hydrocyclones.* Powder. Technol. 427.

HOU, D.X., Zhao, Q, Cui, B.Y, Wei, D.Z., SONG, Z.G., Feng, Y.Q., 2022. *Geometrical configuration of hydrocyclone for improving the separation performance.* Adv. Powder. Technol. 33, 103419,

HSIEH, K.T., RAJAMANI, K., 1988. *Phenomenological model of the hydrocyclone: Model development and verification for single-phase flow.* Int. J. Miner. Process. 22(1-4), 223-237.

JIANG, L.Y., LIU, P.K., ZHANG, Y.K., Li, X.Y., YANG X.H., HOU, D.X., CHEN, B., 2023. *Effect of cone section combination form on the separation performance of a biconical hydrocyclone*, Powder. Technol. 419.

JIANG, L.Y., LIU, P.K., ZHANG, Y.K., Li, X.Y., YANG X.H., Xu, H.L., Wang, H., 2022. *Experimental study of the separation performance of a hydrocyclone with a compound curve cone.* Powder Technol., 409,117829.

JIANG, L.Y., LIU, P.K., YANG, X.H., ZHANG, Y.K., LI, X.Y., XU, H.L., WANG, H., 2020. *Experimental research on the separation performance of W-shaped hydrocyclone.* Powder. Technol. 372, 532-541.

JUNG, K.J., HWANG, I.J., KIM, Y.J., 2019. *Effect of inner wall configurations on the separation efficiency of hydrocyclone.* J. Mech. Sci. Technol. 33(11), 5277-5283.

LEE, W., JUNG, M., HAN, S., PARK, S., PARK, J.K., 2020. *Simulation of layout rearrangement in the grinding/classification process for increasing throughput of industrial gold ore plant.* Miner. Eng. 157, 106545.

LI, C.Y., LI, J.P., WANG, N.N., ZHAO, Q., WANG, P., 2021. *Status of the treatment of produced water containing polymer in oilfields: A review*. J. Environ. 9(4), 105303.

LIU, P.K., FU, W. X., JIANG, L.Y., ZHANG, Y.K., YANG, X.Y., LI, X.Y., WANG, H., 2023. *The separation performance of a parabolic hydrocyclone in separating iron from red mud*. Powder. Technol. 416, 118205.

LIU, P.K., FU, W.X., JIANG, L.Y., YANG, X.H., ZHANG, Y.K., LI, X.Y., ZHANG, Y.L., 2023. *Effect of the position of overflow pipe with mixed spiral structures on the separation performance of hydrocyclones*. Separations. 10(2). 84.

LV, W.J., ZHAO, K.Q., MA, S.H., KONG, L.K., DANG, Z.H., CHEN, J.Q., ZHANG, Y.H., HU, J., 2020. *Process of removing heavy metal ions and solids suspended in micro-scale intensified by hydrocyclone.* J Clean Prod. 263, 116960.

MOTION, A., BENARD, A., 2017. *Design of liquid-liquid separation hydrocyclones using parabolic and hyperbolic swirl chambers for efficiency enhancement.* Chem. Eng. Res. Des. 122: 184-197.

PADHI, M., KUMAR, M., MANGADODDY, N., 2020. *Understanding the Bicomponent Particle Separation Mechanism in a Hydrocyclone Using a Computational Fluid Dynamics Model.* Ind. Eng. Chem. Rec. 59(25): 11621-11644.

PATRA, G.; BARNWAL, R.; BEHERA, S.K.; MEIKAP, B.C., 2018. *Removal of dyes from aqueous solution by sorption with fly ash using a hydrocyclone.* J. Environ. 6(4): 5204-5211.

SONG, T., YAO, Y., NI, L., 2020. *Response surface method to study the effect of conical surface and vortex-finder lengths on de-foulant hydrocyclone with reflux ejector*. Sep. Purif. 253, 117511.

SU, T.L., ZHANG, Y.F., 2022. *Effect of the Vortex Finder and Feed Parameters on the Short-Circuit Flow and Separation Performance of a Hydrocyclone*. Processes. 10(4):771.

TANG B., XU, Y.X., SONG, X.F., SUN, Z., Yu, J.G., 2015. *Numerical study on the relationship between high sharpness and configurations of the vortex finder of a hydrocyclone by central composite design*. Chem. Eng. J. 278, 504–516.

TIAN, T.Y., NI. L, SONG, T., SHEN, T., YAO, Y., ZHAO, J.N., 2019. *Numerical study of foulantwater separation using hydrocyclones enhanced by reflux device: effect of underflow pipe diameter*. Sep. Purif. Technol. 215, 10–24.

VYSYARAJU, R., PUKKELLA, A.K., 2022. *Computational investigation of a novel hydrocyclone for fines bypass reduction*. Powder Technol. 395, 501-515

VEGA-GARCIA, D., BRITO-PARADA, P.R., CILLIERS, J.J., 2018. *Optimising small hydrocyclone design using 3D printing and CFD simulations*. Chem. Eng. J. 350, 653–659.

XIE, H.Y., SUN, R., REN, X.J., YOU, Z.C., LIU, Y.H., FENG, D.X., CHEN, L.Z., 2020. *Development of a novel fluidized hydrocyclone concentrator for mineral separation*. Sep. Purif. 248, 116960.

YANG, Q., WANG, H.L., LIU, Y., ZHI, M.L., *Solid/liquid separation performance of hydrocyclones with different cone combinations*. Sep. Purif. Technol. 74 (3) (2010) 271–279.

YE, J.X., XU, Y.X., SONG, X.F., YU, J.G., 2019. *Novel conical section design for ultra-fine particles classification by a hydrocyclone.* Chem. Eng. Res. Des. 144: 135-149.

ZHANG, H., NI, H.J., 2022. *Design and numerical simulation on new type near-bit hydrocyclone for downhole olid-Liquid Separation.* Arab. J. Sci. Eng. 47(9): 11941-11951.

ZHANG, L., YANG, L., HOU, H.C., ZHAO, Y; LIN, J., ZHANG, Z.L., BU, C.Y., ZHENG, X.R., FU, D., 2023. *Experimental study of quartz classification in the enhanced gravity field using Falcon concentrator*. Physicochemical Probl Mi. 59(6).